[Article ID] 1003- 6326(2002)04- 0615- 06

Microstructure evolution in a large-grained TiAl alloy①

SUN Feng(孙 锋), LIN Dong-liang(林栋樑)
(School of Materials Science and Engineering,
Key Laboratory of Ministry of Education for High Temperature Materials and Tests,
Shanghai Jiaotong University, Shanghai 200030, China)

[Abstract] Microstructure evolution during superplastic deformation of a large-grained TiAl alloys with near-γ microstructure was characterized by orientation imaging microscopy (OIM) and transmission electron microscopy (TEM). In OIM, significant grain refinement is observed at different strain levels with an increase in the density of low angle grain boundaries and high angle grain boundaries. A direct evidence of dynamic formation of grain boundaries with misorientation of 15°~ 30° during deformation is found, which is a result of subboundary evolution. The formation of subboundaries by intersecting dislocations, and the evidence of dislocation glide in the interior of grains are revealed by TEM observations. A continuous recovery and recrystallization process similar to that in FeAl and Fe_3Al is proposed as superplastic deformation mechanism in the large-grained TiAl alloy.

[Key words] TiAl alloy; superplasticity; microstructure evolution; large-grained; EBSP
[CLC number] TG 146.2 [Document code] A

1 INTRODUCTION

A continuous recovery and recrystallization mechanism[1,2] was proposed by Lin and coworkers for the superplasticity in large-grained FeAl and Fe_3Al alloys[1~4] which exhibit usual flow characteristics of conventional fine-grained super- plastic materials, without the prerequisites of a fine grain size for the occurring of grain boundary sliding (GBS). The model is based on the dynamic formation and evolution of unstable subgrain boundaries (SGB), in that, appropriate dislocation motion velocity and obstacles are needed to construct and maintain SGB. It can be inferred that large-grained superplasticity should be common in most intermetallics having an intrinsically low dislocation mobility. This inference has been partially proved. Recently, superplastic phenomena in large-grained TiAl[5] and NiAl[6] alloys were observed in our laboratory. Other workers also reported similar phenomena in Fe_3Si[7] and NiAl[8] alloys, although there still have different viewpoints.

A detailed microstructure characterization for a superplastic deformed γ-TiAl alloy with initially large grains was presented, which has been reported in our previous work[5]. Superplastic phenomenon was found in the regime of 1025~ 1100 ℃ and 4×10^{-5} ~ $1.28\times10^{-3}s^{-1}$ with a maximum elongation close to 290% and a maximum strain rate sensitivity index of 0.39, in that the reduction of average grain size after deformation similar to FeAl and Fe_3Al was observed. In this paper, transmission electron microscopy and orientation imaging microscopy are utilized to explore the microstructure evolution during and after deformation. Then, combined with previous work in FeAl and Fe_3Al, the mechanism of superplastic deformation is discussed.

2 EXPERIMENTAL

Starting material was a near-γ TiAl alloy of nominal composition Ti-47Al-2Mn-2Nb-1B (mole fraction, %). Tensile specimens with gauge section of 8 mm × 4 mm × 1.3 mm were prepared. The specimens were superplastically deformed to different strains at 1075 ℃ (then water quenched) using a initial stain rate of $1.6\times10^{-4}s^{-1}$. As a contrast, a test temperature of 1025 ℃ was also used. Samples for analyses were sectioned from the gage section of specimens. Some for orientation imaging microscopy (OIM) were electropolished following a sequence of mechanical grinding and polishing. Other samples were ground to about 70 μm, then thinned electrolytically by standard twin-jet method to gain TEM foils. The electrolyte was a 5% perchloric acid solution in methanol, common for OIM and TEM. The temperature and voltage were kept at about - 40 ℃ and 30 ~ 40 V, respectively.

OIM analyses were performed on specimens deformed to 30%, 98%, 170% and 80% (only for 1025 ℃). Automatic generation and indexing of electron back-scattered diffraction patterns (EBSPs) were carried out on an orientation imaging microscope produced by HKL Technology Inc, Denmark, which equipped a back-scattered electron detector and Chan-

① [Foundation item] Project (59895150) supported by the National Natural Science Foundation of China
[Received date] 2001- 10- 08

nel 4 analysis software. Beam scan mode was adapted with a step spacing of 1 μm over an area of 115 μm × 115 μm~ 161 μm × 161 μm. The image of microstructure was reconstructed by creating grain boundary maps from the EBSP measurements. Designation of grain boundaries was based on a grain boundary criteria, ω, given by the researcher. Misorientation angle θ is calculated between grid points in the scan field and compared with ω. In the paper, three criteria, $2° < \omega < 10°$, $10° \leqslant \omega < 15°$ and $\omega \geqslant 15°$ were considered. By employing these criteria during the generation of the grain boundary maps, different images of the microstructure were constructed.

3 RESULTS AND DISCUSSION

3.1 Deformation microstructure

Fig. 1 exhibits EBSD orientation mapping images of deformed specimens based on the grain boundary criteria, in which (a) ~ (c) correspond to strain of 30%, 98%, 170% at 1075 ℃, respectively, and (d) to that of 80% at 1025 ℃. In these maps, white lines represent grain boundary with a misorientation angle θ higher than 15°, which should be high-angle grain boundary (HAGB). Gray lines represent grain boundaries with misorientation angles (θ) of 10° ~ 15°, whereas black lines for θ between 2° and 10°, which should be low-angle grain boundaries (LAGBs). It clearly shows grain refinement, and the increase in the amount of low-angle grain boundary during deformation. At the deformation of 30%, corresponding to a true strain of 0.26%, a few LAGBs were shown in the microstructure, and they distributed mainly in the adjacent areas of HAGB. It should clarify the fact that the superplasticity in large-grained TiAl alloy is not originated by the pre-existing subgrains before deformation. When the strain is increased up to 98%, the microstructure displays many LAGBs, which shows two different distribution morphologies, one is distributed uniformly in some areas which should be in the original large grains; another is similar to 30% deformed specimens, distributed near to HAGBs, whose areas should be in newly formed grains or recrystallized grains. Similar characteristic was observed in 170% deformed specimens (as shown in Fig. 1(c)) and 80% deformed specimens at 1025 ℃ (Fig. 1(d)). Another outstanding characteristic is the significant increase in the amount of HAGBs and small areas enclosed by HAGBs with increasing strain. It should be pointed out, not all HAGBs depicted are ordinary grain boundaries, some are twin boundaries, so an area

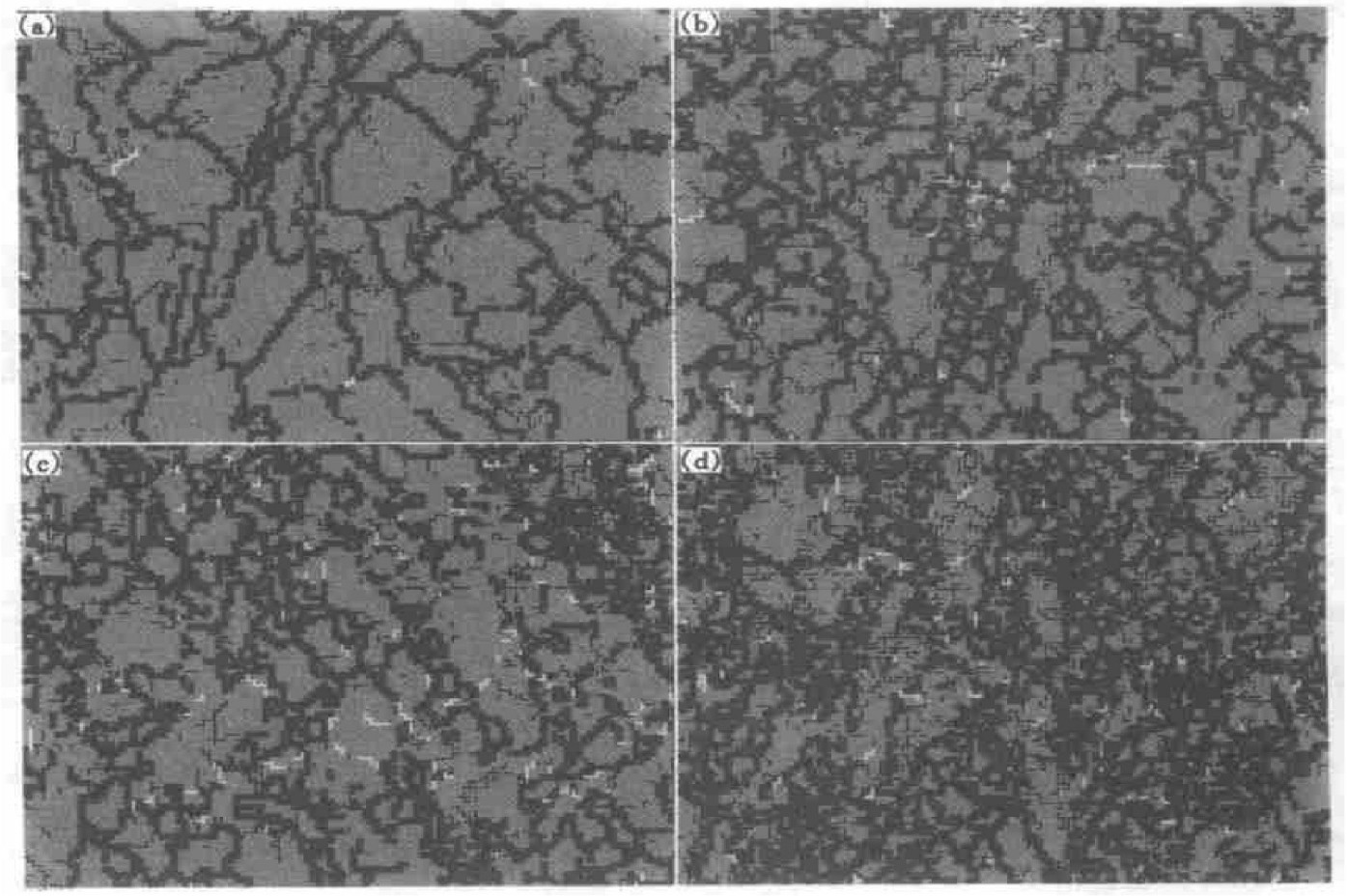

Fig. 1 Orientation mapping images of deformed specimens under different strains at an initial strain rate of $1.6 \times 10^{-4} s^{-1}$

(a) —30%; (b) —98%; (c) —170%; (d) —80%. (a) ~ (c) —Deformed at 1075 ℃; (d) —Deformed at 1025 ℃

enclosed by HAGBs may be a part of a single grain, that is why the grain size is smaller than that observed by optical microscopy.

When comparing the microstructure of deformed specimens at different temperatures, it is clearly shown that the grain refinement is more significant at lower temperature, in which a high density of LAGBs and HAGBs can be observed. The superplasticity at 1025 ℃ is more inferior to 1075 ℃, which suggests that a slowly reduction of grain size is needed to maintain superplastic flow, in other words, to keep the superplastic mechanism in effect.

3.2 Misorientation distribution

Fig. 2 shows the distribution of misorientation angles in deformed microstructure presented in Fig. 1, which is expressed as relative frequency in total points. The correlated plot displays the misorientation data between neighboring points in an orientation map; whereas an uncorrelated plot shows the misorientation between randomly chosen points in the data set. In the correlated data, a minimum angle of 1° was chosen for statistics. In addition, the data at θ = 85°~ 90° have been filtered out, which are abnormally high and have no large variations in different specimens. It is believed to be caused by anti-phase domain boundaries.

All the maps show a high fraction of misorientation angle at θ= 1°~ 5°, by compared with a map with a minimum angle of 2° (as shown in Fig. 2(a)), it can be found that the high fraction are mainly contributed by θ= 1°~ 2°. This part is difficult to do quantitative analysis due to the resolution limit of 2°. At the deformation of 30%, the correlated distribution shows a lack of grain boundaries with misorientation of 15°~ 30°, which can be seen in the uncorrelated distribution. Besides that, the fraction of LAGBs with θ= 5°~ 10° is very low when compared with HAGBs and boundaries with θ< 5°. In addition, the fraction of boundaries with θ= 10°~ 15° is very low, too, as seen in the orientation mappings of Fig. 1. It is a significant feature of observed microstructure, which suggests the original microstructures only have HAGBs with misorientation angles above 30°, and a strain of 30% is not enough to form uniform substructure. In other words, most immobile dislocations still exist in the form of dislocation walls and LAGBs with θ< 5° at such a deformation level. It is consistent with our previous research that apparent strain softening occurs at a true strain of about 0.4[5].

With increasing strain, the fraction of LAGBs with θ= 5°~ 10° increased, and more prominently, the grain boundaries with θ= 15°~ 30° appeared, which also increased with the strain. The fraction of grain boundaries with θ= 10°~ 15° increased when strain increased to 98%, but changed very little between the strain of 98% and 170% (or it could be

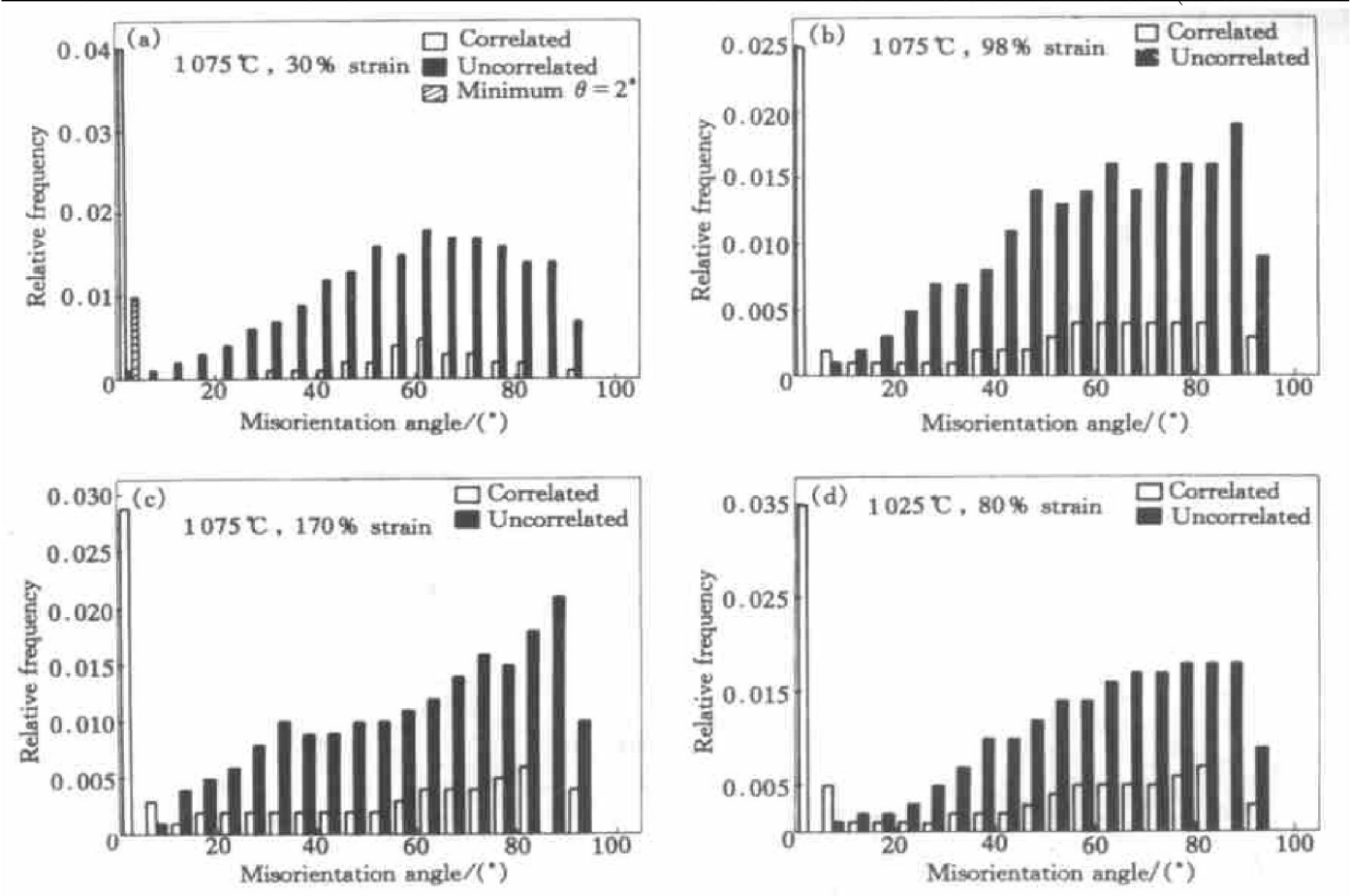

Fig. 2 Distribution of misorientation angles in deformed microstructure presented in Fig. 1
(a) —30%; (b) —98%; (c) —170%; (d) —80% (1025 ℃)

considered to remain constant). This phenomenon was resulted only from the evolution of subboundaries. During deformation, LAGBs with $\theta < 10^\circ$ transformed continuously to those with $\theta > 10^\circ$, so the fraction of grain boundaries with $\theta > 10^\circ$ increased; while the grain boundaries with $\theta = 10^\circ \sim 15^\circ$ were extremely unstable, having a strong tendency to transform into HAGBs. At large strain, a dynamical balance will be reached between the evolution of LAGBs from $\theta < 10^\circ$ towards $\theta > 10^\circ$, and the evolution from $\theta = 10^\circ \sim 15^\circ$ towards $\theta > 15^\circ$, then the fraction of LAGBs with $\theta = 10^\circ \sim 15^\circ$ will keep constant.

Distribution of misorientation angles at high angle, above 30°, also shows a change during deformation, that is, at initial stage of deformation, the fraction of HAGBs around $\theta = 60^\circ$, which should be twin boundaries, was highest. As deformation grew up, the fraction of 60° HAGB decreased; while other HAGBs, especially those with $\theta > 75^\circ$, increased rapidly. Finally, when strain up to 170%, a maximum peak appeared at $\theta = 80^\circ \sim 85^\circ$. Such a change corresponded to the formation of new grains and the wipe-off of original twin boundaries.

At lower temperature such as 1025 ℃, in the specimen deformed to 80%, a higher density of LAGBs was observed, while the distribution of HAGBs is similar to that deformed to 170% at 1075 ℃. It suggests dislocation substructures at lower temperature show stronger tendency to form LAGBs, and to transform to HAGBs.

3.3 TEM results

TEM images of substructure in the deformed samples are shown in Fig. 3. As can be seen, well-developed subgrains and deformation twins across subgrain boundary were observed in the original γ grains. Dislocation arrays and networks in subgrain boundary, dislocation tangles and long segments, also including micro-twins, which increase with strain, constituted the main deformation substructure in the equiaxed γ grain. It is noticed that subgrains in Fig. 3(c) were elongated significantly, which is a typical characteristic of dislocation glide, and also a signal of unaccommodating deformation. In contrast with the high density in subgrain boundaries, the dislocation density is low in the interior of grains, which is consistent with our simulated result in an order of $10^{11} \sim 10^{12}\ m^{-2}$ [9]. It suggests that at the steady-state (or quasi steady-state) flow stage, the dislocations in grain will remain a relatively low density due to the formation of subgrain boundaries, coupled with the absorption by subboundaries, i.e, dislocations are annihilated by recovery process with subgrain evolution instead of by dynamic recrystallization prevailed in creep of TiAl alloys[10].

Fig. 4 shows a forming subgrain boundary. As pointed out by label *A*, two dislocations intersect and react with each other, and rearrange to form the subboundary. It is interesting to view that the dislocations at *A* are originated from the pile-ups of dislocations in front of the original grain boundary labelled as *B*. It seems that the dislocation pile-ups are favourable to form subboundary.

In Fig. 5, a series of TEM micrographs were used to identify dislocation characteristics in the subgrain boundary labelled as *C* in Fig. 4. As seen from Fig. 5(a), at operating vector $\boldsymbol{g} = \bar{2}20$, the subboundary shows a dislocation net, which was composed by two sets of intersecting dislocation arrays. When $\boldsymbol{g} = \bar{1}11$ and $\boldsymbol{g} = \bar{1}11$, one set of two dislocation arrays is invisible, alternately. At $\boldsymbol{g} = 020$, two arrays become all invisible. Using the $\boldsymbol{g} \cdot \boldsymbol{b} = 0$ criteria for the invisibility of dislocations (where $\boldsymbol{b}$ is the Burger vector), it is easily to deduce that the subgrain boundary is composed by [101] and [$10\bar{1}$] type superdislocations. There is no visible dissociation

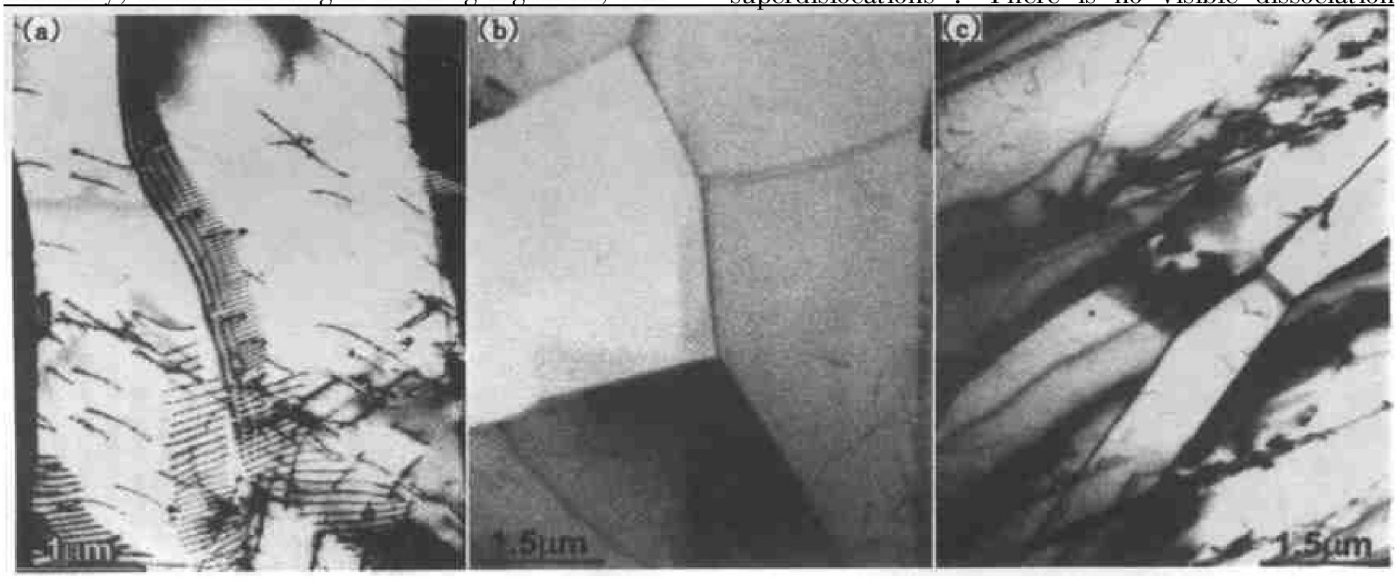

Fig. 3 Typical substructures after deformation of TiAl alloy at 1075 ℃ and $1.6 \times 10^{-4}\ s^{-1}$
(a) —Deformed to 60%; (b) —Deformed to 98%; (c) —Deformed to 170%

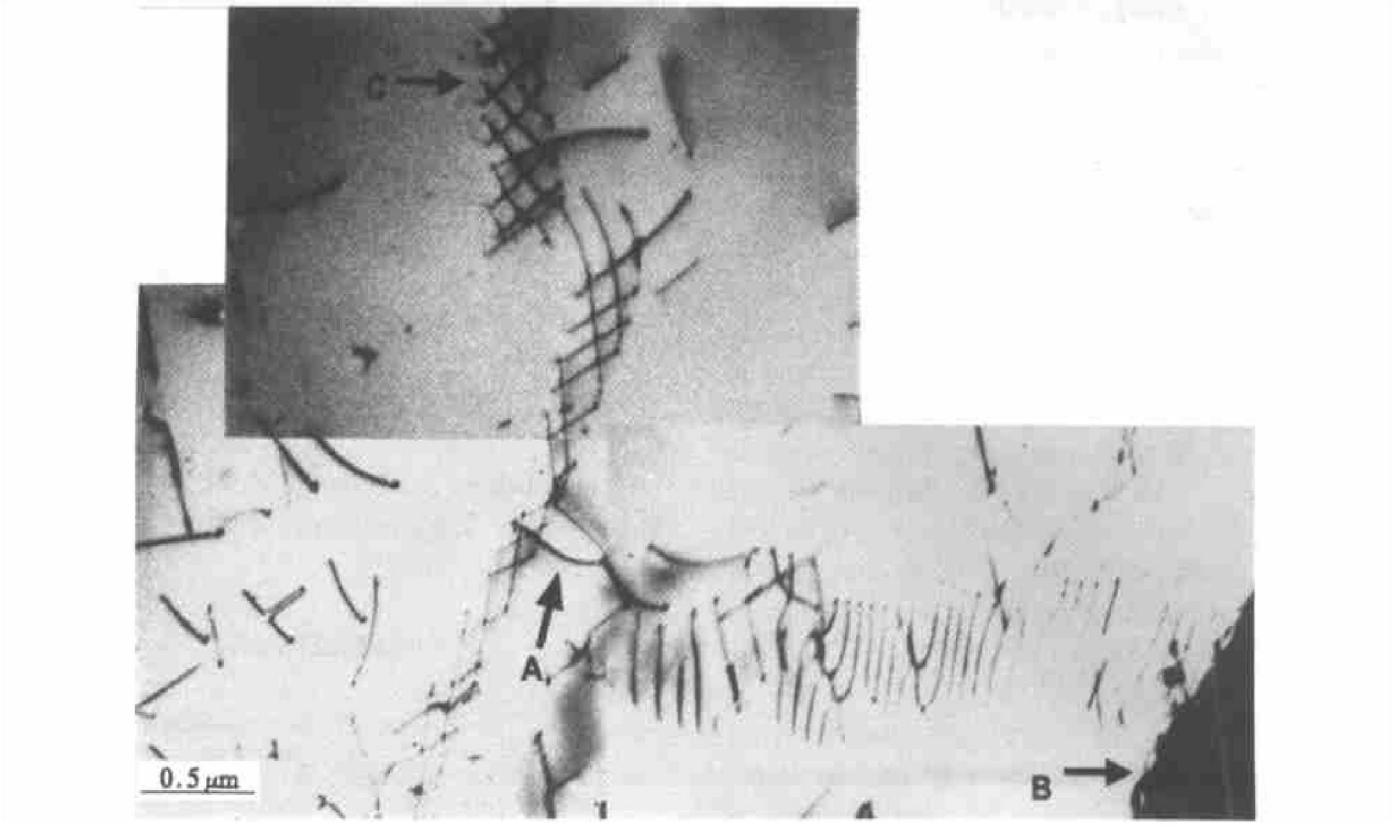

Fig. 4 Bright field (BF) electron micrograph showing a forming subboundary and dislocation pile-ups in front of an original grain boundary (1 075 ℃, $1.6 \times 10^{-4} s^{-1}$, deformed to 60%)

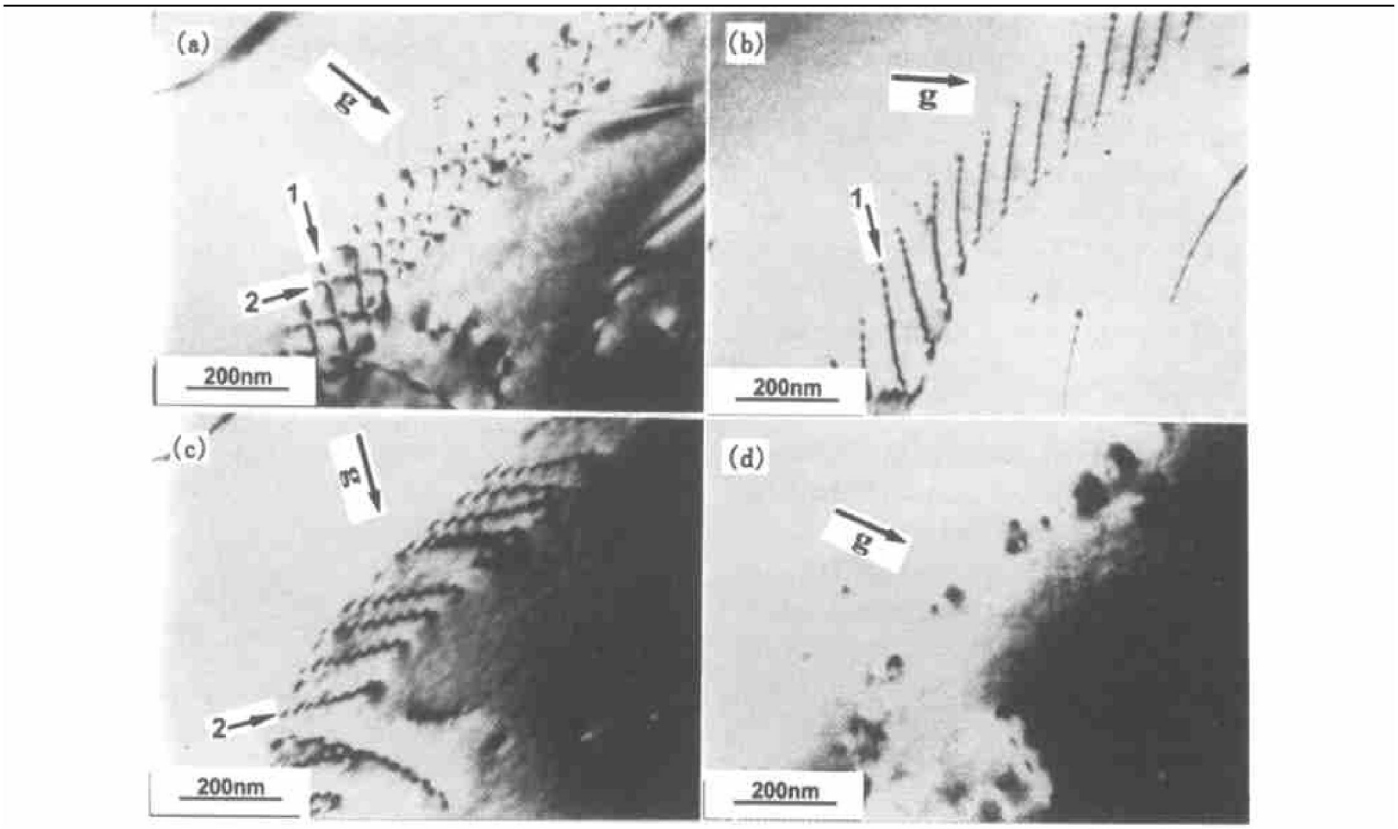

Fig. 5 Diffraction contrast analysis of dislocation substructure in subgrain boundary
(a) $-\boldsymbol{g}=\bar{2}20$, $\boldsymbol{B}=[110]$; (b) $-\boldsymbol{g}=\bar{1}11$, $\boldsymbol{B}=[110]$; (c) $-\boldsymbol{g}=\bar{1}1\bar{1}$, $\boldsymbol{B}=[110]$; (d) $-\boldsymbol{g}=020$, $\boldsymbol{B}=[101]$

of superdislocations to be observed. Apart from the $[101]$ and $[10\bar{1}]$ type dislocations, other type dislocations are rare to find. The interaction between dislocations and subgrain boundaries, and the evolution of subgrain boundaries are still inexplicit.

3.4 Discussion

As reported in our previous work[5], the flow behaviour in superplastic deformation of the large-grained TiAl alloy is similar to those in conventionally superplastic alloys. But there exist some significant

differences in microstructural evolution and mechanism between the large-grained TiAl alloy and conventionally fine grained superplastic material. At first, superplastic behaviour was found in the large-grained TiAl alloy without the usual prerequisites of a fine grain size and grain boundary sliding[11]. Moreover, the metallographic examinations have shown that the average grain size of the large-grained TiAl alloy decreased during superplastic deformation and a much finer grain size could be obtained after superplastic deformation; while in fine-grained superplastic alloys the grain size keeps nearly constant or have a little growth. The phenomenon of grain refinement is confirmed further by OIM studies. As view the fact of subgrain formation, high density of LAGBs and dynamic formation of HAGBs, it is obviously that a recovery and recrystallization process appeared during superplastic deformation in the large-grained TiAl alloy.

Compared with the superplastic phenomenon in large-grained FeAl and Fe_3Al alloys[1~4], the large-grained TiAl alloy shows similar characteristics of subgrain evolution during deformation. So it is reasonable to deduce that there exists a superplastic mechanism similar to FeAl and Fe_3Al in large-grained TiAl, although the latter is more complex due to the existence of twin boundaries and anti-phase domain boundaries. TiAl alloys are subject to mechanical twinning due to elastic incompatibilities. Besides the effect of accommodate deformation, the role of deformation twin is still uncertain, which should be as dislocation sources, or as effective obstacles to help subgrain boundaries to form. In this consideration, deformation twinning may insert a beneficial effect while it is harmful in the case of fine-grained superplasticity[12].

A common characteristic observed in TiAl, FeAl and Fe_3Al, and also in Fe_3Si alloys is that subgrains form preferentially at adjacent areas of HAGBs, which is reasonable due to stress concentration usually occurred at corners or triple junctions of HAGBs. Such a fact suggest original GBs have effects on the formation of subgrains, in further on superplastic deformation, so the effects of grain size has to be considered even for large-grained superplasticity.

As a brief description, the superplastic mechanism in large-grained TiAl alloy is a process of continuous recovery and recrystallization. The gliding dislocations intersect and react with each other and arrange themselves as dislocation arrays or networks to form subboundaries with the aid of dislocation climb, while the deformation twinning playing a role of deformation accommodation and dislocation sources. During deformation, gliding dislocations can be trapped and absorbed by subboundaries, and then subboundaries evolve continuously towards LAGBs, in further, HAGBs. Such a process should continuously occur till the average grain size is close to the subgrain size. A constant dislocation density in the interior of grains is maintained under a constant stress at a given temperature, which corresponds to the steady-state flow stage of superplastic deformation.

ACKNOWLEDGEMENT

The authors would like to thank Prof Q Liu and Mr J Meng of Tsinghua University for help on EBSD experiments.

[REFERENCES]

[1] Lin D, Shan A, Chen M. Superplasticity in large-grained Fe_3Al alloys [J]. Intermetallics, 1996, 4: 489- 496.

[2] Lin D, Li D, Liu Y. Superplasticity in large-grained FeAl based intermetallic alloys [J]. Intermetallics, 1998, 6: 243- 256.

[3] Lin D, Shan A, Li D. Superplasticity in Fe_3Al-Ti alloy with large grains [J]. Scripta Metall Mater, 1994, 31: 1455- 1460.

[4] Li D, Shan A, Liu Y, et al. Study of superplastic deformation in a FeAl based alloy [J]. Scripta Metall Mater, 1995, 33: 681- 685.

[5] Sun F, Lin D. Superplastic phenomenon in a large-grained TiAl alloy [J]. Scripta Mater, 2001, 44: 665- 670.

[6] Jiang D, Lin D. Superplasticity of single-phase Ni-40Al intermetallics with large grains [J]. Journal of Mater Sci Letters, 2002, 21: 505- 508.

[7] Hanada S, Kim W Y, Yoshimi K, et al. Superplasticity in intermetallics [A]. Chandra T, Sakai T. THERMEC' 97, International Conference on Thermomechanical Processing of Steels & Other Materials [C]. Wollongong, Australia. TMS, 1997, 1883- 1889.

[8] Du X H, Guo J T, Zhou B D. Superplasticity of stoichemical NiAl with large grains [J]. Scripta Mater, 2001, 45: 69- 74.

[9] Sun F. A Study on the Large-grained Superplasticity in TiAl and Fe_3Al Intermetallics [D]. Shanghai: Shanghai Jiaotong University, 2002. 37- 44.

[10] Skrotzki B. A new microstructural view of creep in near γ TiAl alloys [J]. Key Engineering Materials, 2000, 171- 174: 701- 708.

[11] Likhachev V A, Myshalyaev M M, Olevskii S S, et al. Superplasticity and structure of aluminium [J]. Acta Metall, 1974, 22: 829- 834.

[12] Imayev R, Gabdullin N, Salishchev G. Effect of grain size on superplasticity of an intermetallic Ti_3Al compound [J]. Intermetallics, 1997, 5: 229- 236.

(Edited by YANG Bing)